Carambola-like Bi_2Te_3 superstructures with enhanced photoabsorption for highly efficient photothermal therapy in the second biowindow

Ying Zhao,[a,b] Yang Liu,[a,b] Qishun Wang,[c] Jianhua Liu,[d] Songtao Zhang,[a] Tianqi Zhang,[d] Daguang Wang,[e] Yinghui Wang,*,[a] Longhai Jin,*,[d] and Hongjie Zhang*,[a,b,c]

a. State Key Laboratory of Rare Earth Resource Utilization, Changchun Institute of Applied Chemistry (CIAC), Chinese Academy of Sciences, Changchun 130022, China.

b. University of Science and Technology of China, Hefei 230026, China.

c. Department of Chemistry, Tsinghua University, Beijing 100084, China.

d. The second hospital of Jilin University, Changchun 130041, China.

e. Department of Gastric and Colorectal Surgery, the First Hospital, Jilin University, Changchun, Changchun 130021, China.

E-mail: yhwang@ciac.ac.cn (Y. Wang), jinlonghai@jlu.edu.cn (L. Jin), hongjie@ciac.ac.cn (H. J. Zhang).

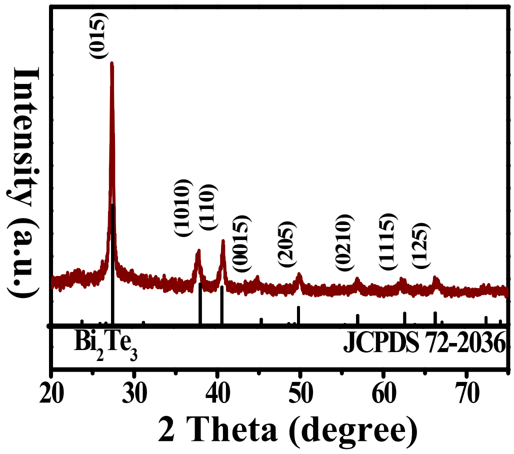

Fig. S1. XRD spectrum of Bi_2Te_3.

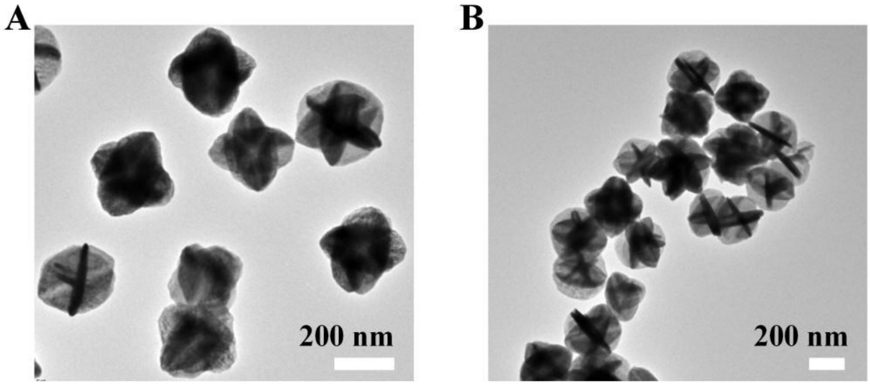

Fig. S2. TEM images of Bi_2Te_3@PEG.

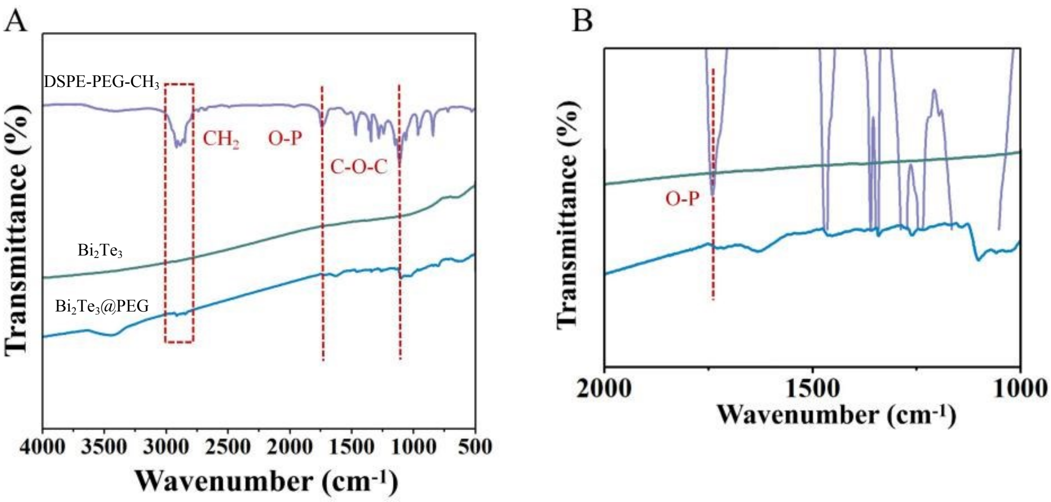

Fig. S3. (A) FT-IR spectra of DSPE-PEG-CH_3, Bi_2Te_3, and Bi_2Te_3@PEG. (B) Partial enlargement of Fig. A (1000-2000 cm^{-1}).

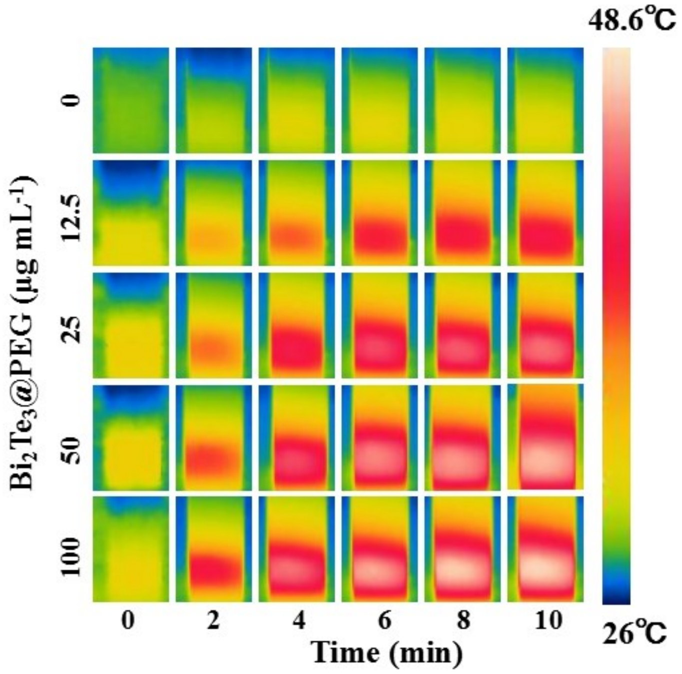

Fig. S4. Infrared thermal images of Bi_2Te_3@PEG aqueous solutions irradiated with an 1064 nm laser (1 W cm^{-2}) from 0 to 10 min at varied concentrations (0, 12.5, 25, 50, 100 ppm).

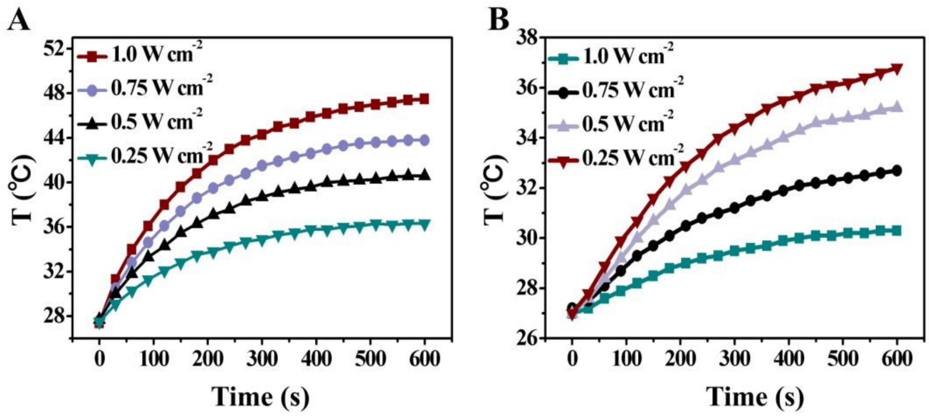

Fig. S5. (A) Temperature curves of Bi_2Te_3@PEG (100 ppm) under the irradiation of 1064 nm laser with different power density (1, 0.75, 0.5, 0.25 W cm^{-2}). (B) Temperature curves of Bi_2Te_3 nanoparticles (100 ppm) under the irradiation of 1064 nm laser with different power density (1, 0.75, 0.5, 0.25 W cm^{-2}).

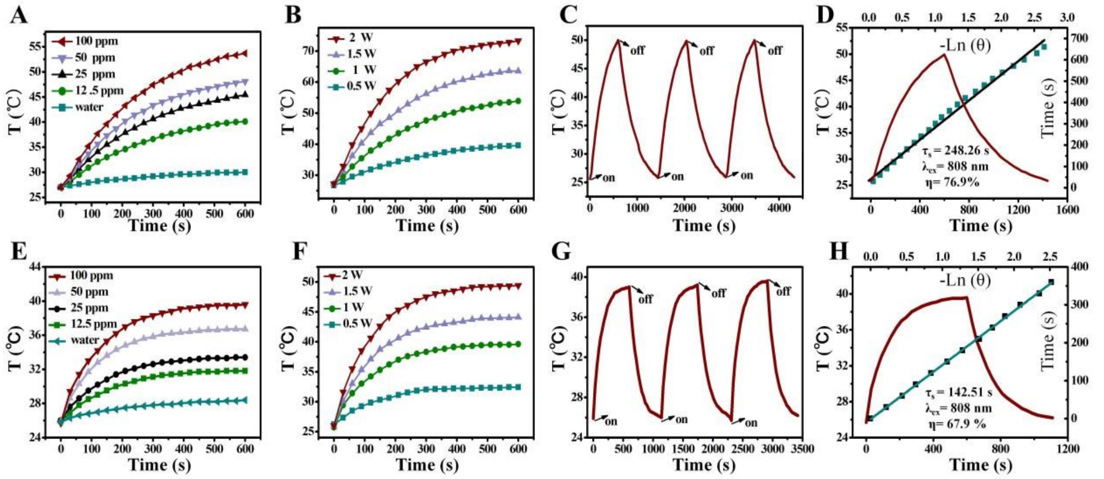

Fig. S6. (A) Temperature rise of Bi_2Te_3@PEG with different concentrations (0, 12.5, 25, 50, 100 ppm) under the irradiation of 808 nm laser (1 W cm^{-2}). (B) Temperature curves of Bi_2Te_3@PEG (100 ppm) under the irradiation of 808 nm laser with different power density (1, 0.75, 0.5, 0.25 W cm^{-2}). (C) Temperature of Bi_2Te_3@PEG over three on/off cycles of 808 nm laser. (D) Heating and cooling curves of Bi_2Te_3@PEG, linear time data acquired from the cooling period. (E) Temperature rise of Bi_2Te_3 nanoparticles with different concentrations (0, 12.5, 25, 50, 100 ppm) under the irradiation of 808 nm laser (1 W cm^{-2}). (F) Temperature curves of Bi_2Te_3 nanoparticles (100 ppm) under the irradiation of 808 nm laser with different power density (1, 0.75, 0.5, 0.25 W cm^{-2}). (G) Temperature of Bi_2Te_3 nanoparticles over three on/off cycles of 808 nm laser. (H) Heating and cooling curves of Bi_2Te_3 nanoparticles, linear time data acquired from the cooling period.

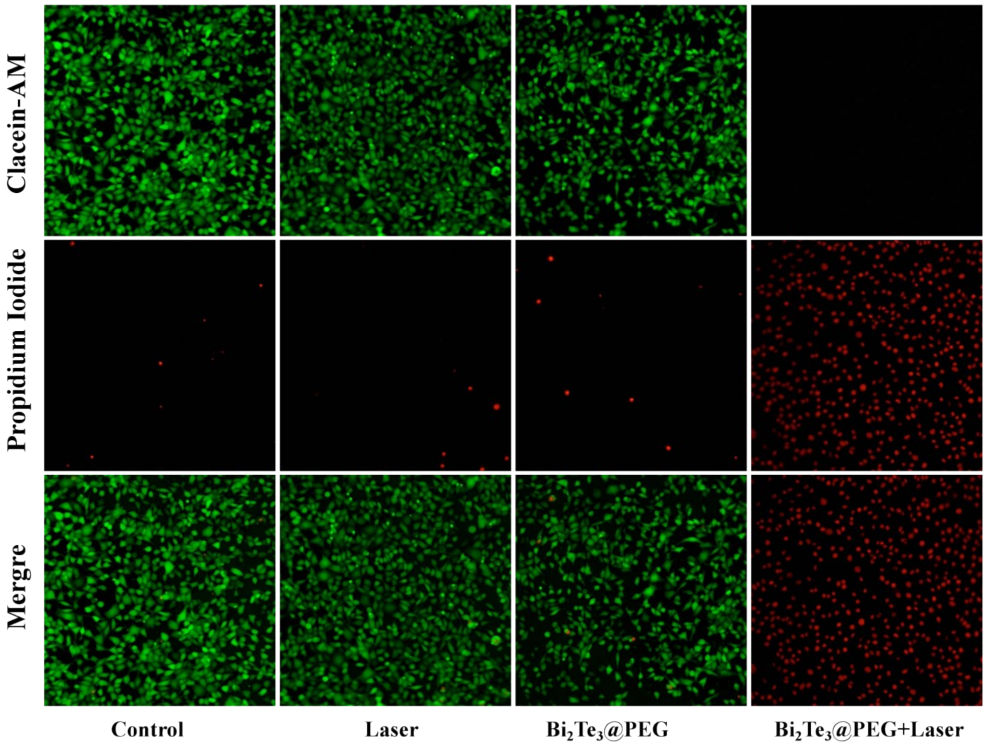

Fig. S7. Fluorescence images of L929 cells in different groups.

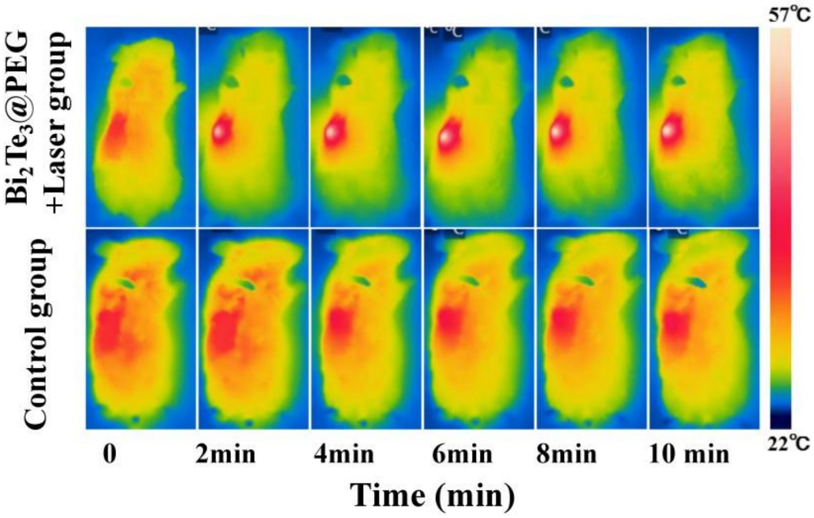

Fig. S8. In vivo thermal imaging of mice after treatment with (a) Bi_2Te_3@PEG + 1064 nm and (b) control (saline + 1064 nm).

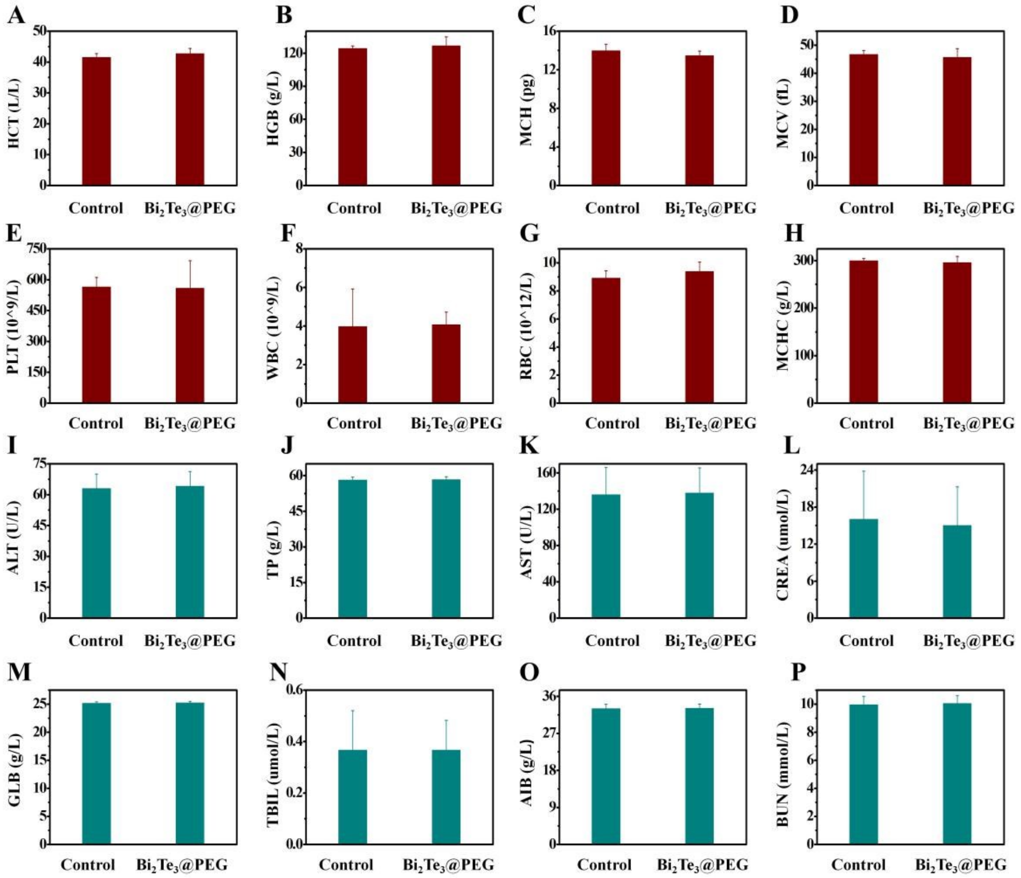

Fig. S9. (A-H) Hematological index and (I-P) biochemical blood analysis of the mice after intravenous injection of Bi_2Te_3@PEG at 30 d.